

Micro-CT Synthesis and Inner Ear Super Resolution via Bayesian Generative Adversarial Networks

Hongwei Li^{1*}, Rameshwara G. N. Prasad^{1*}, Anjany Sekuboyina¹, Chen Niu², Siwei Bai³, Werner Hemmert³, and Bjoern Menze¹

Abstract—Existing medical image super-resolution methods rely on pairs of low- and high- resolution images to learn a mapping in a fully supervised manner. However, such image pairs are often not available in clinical practice. In this paper, we address super resolution problem in a real-world scenario using unpaired data and synthesize linearly eight times higher resolved Micro-CT images of temporal bone structure, which is embedded in the inner ear. We explore cycle-consistency generative adversarial networks for super-resolution task and equip the translation approach with Bayesian inference. We further introduce *Hu Moment* the evaluation metric to quantify the structure of the temporal bone. We evaluate our method on a public inner ear CT dataset and have seen both visual and quantitative improvement over state-of-the-art deep-learning based methods. In addition, we perform a multi-rater visual evaluation experiment and find that trained experts consistently rate the proposed method highest quality scores among all methods. Implementing our approach as an end-to-end learning task, we are able to quantify uncertainty in the unpaired translation tasks and find that the uncertainty mask can provide structural information of the temporal bone.

I. INTRODUCTION

High-quality image guided surgery has allowed clinicians to develop safe and less invasive surgical procedures despite the large inter-individual anatomical variability. Clinical computed tomography (CT) is the common imaging technique for this purpose. However, when delicate structures need to be resolved, as it is the case for example for the insertion of cochlear implant electrodes into the inner ear, a much higher resolution would be desirable. Micro computed tomography (micro-CT) can provide high resolution (HR) images that captures much more details of the human cochlear anatomy, however, it cannot be applied clinically due to the high amount of radiation dose required and due to the limited probe size which fits into the scanners. It is therefore highly clinically relevant to estimate detailed anatomical structures from low-resolution CT using image enhancement or super resolution (SR) techniques.

1) *Related Work*: In recent years, deep learning methods have been introduced to build a mapping function from LR patches to HR patches to solve various SR tasks [12], [13], [16] and achieve superior results over traditional SR methods [2], [15], [1]. Most of the existing deep-learning based SR

methods rely on pairs of LR-HR images to train a network in a fully supervised manner. By downsampling the HR images to generate spatially-aligned LR images, the paired images for the input of deep neural network can be easily obtained. However, this strategy often fails to introduce real-world characteristics from the LR domain and therefore struggles to generalize when given real low-resolution input. As a consequence, the models trained on simulated data become less effective when applied to practical scenarios when there exists a large domain shift between LR and HR domains. Especially in the SR task from clinical CT (LR) to Micro-CT (HR), noise, voxel size and sensor types result in large domain gap which make it extremely difficult to generate paired LR-HR images. Recently, generative adversarial networks (GANs) and their extensions [6], [20], [3] have been proposed to learn the data distribution from either paired or unpaired datasets. Although unpaired image-to-image translation using GANs has been recently explored in medical imaging [10], [19], it cannot be directly applied to SR tasks because the translation process does not learn to adapt voxel size. Meanwhile, a sufficient image quality cannot be easily guaranteed as the synthetic images lie in the latent space. To the best of our knowledge, this work is the first to explore GANs for *real-world* SR tasks and quantify model uncertainty in unsupervised image translation.

2) *Contributions*: 1) We propose a GANs-based approach to solve the unpaired super resolution problem in a clinical scenario and incorporate Bayesian inference to quantify model uncertainty to guarantee applicability in a translation to real world problems. 2) We provide both qualitative and quantitative results on synthesis of Micro-CT, showing the superiority of our method over state-of-the-art. 3) We present results of multi-rater visual evaluation, performed by three experienced otolaryngology researchers who confirm the superior quality of synthetic images while outperforming state-of-the-art approaches.

II. METHODS

Our super resolution approach includes two main components: 1) Unpaired image-to-image translation network and 2) Bayesian inference as shown in 1.

A. Problem definition

The goal of the super resolution task is to map a low-resolution (LR) domain to a high-resolution (HR) domain. Let \mathcal{L} denote a LR image space and \mathcal{H} a HR image space. We assume that \mathcal{L} and \mathcal{H} are not paired in a common clinical

* equal contributions.

H. Li, R. Prasad, A. Sekuboyina and B. Menze are with Department of Computer Science, Technical University of Munich, Germany; C. Niu is with the Department of Medical Imaging, First Affiliated Hospital of Xi'an Jiaotong University, Xi'an, China; S. Bai and W. Hemmert are with Department of Electrical and Computer Engineering and Munich School of BioEngineering, Technical University of Munich, Garching, Germany.

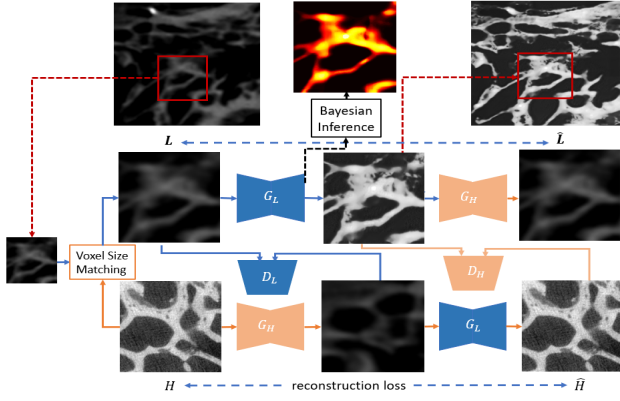


Fig. 1: Method overview. We upsample the input LR images by bicubic interpolation to match the voxel size. Then we sample local patches from these upsampled slices of CT scans. Then the unpaired LR and HR image patches are fed into a cycle-consistency generative adversarial network to perform the super resolution task. Finally Bayesian inference is performed to estimate the model uncertainty given a patch.

setting. Considering the complexity of imaging datasets, we claim that it is difficult to introduce LR domain characteristics in medical datasets by traditional techniques such as, interpolation and noise injection [17], which restrict the applicability of SR techniques. Thus we aim to learn a direct mapping from LR domain to HR domain $\Phi : \mathcal{L} \rightarrow \mathcal{H}$ by learning the individual underlying distributions.

B. Patch-Based Unpaired Image Translation

The super-resolution task includes two aspects: 1) Structure enhancement and 2) Image style transfer. We deploy generative adversarial networks to learn the individual underlying distributions including generator networks and discriminator networks. Since it is an unpaired image-to-image translation task, we adapt a cycle-consistency GAN inspired by [20] to handle the unpaired issue. This includes a pair of generators $\{G_L, G_H\}$ and a pair of domain discriminators $\{D_L, D_H\}$. As illustrated in Figure 1, generator G_L aims to translate patches from LR to HR while generator G_H aims to translate from HR to LR. Discriminators $\{D_L, D_H\}$ are trained to distinguish if the generated patches are real or fake in the two domains respectively. In a min-max game, the generators try to fool the discriminators by good image translation. The detailed training losses are as follows:

a) *Self-reconstruction loss*::

$$\mathcal{L}_{rec} = \mathbb{E}_{x \sim \mathcal{L}} [\|x - G_H(G_L(x))\|_1] + \mathbb{E}_{y \sim \mathcal{H}} [\|y - G_L(G_H(y))\|_1] \quad (1)$$

b) *Adversarial loss*::

$$\begin{aligned} \mathcal{L}_{adv} = & \mathbb{E}_{x \sim \mathcal{L}, y \sim \mathcal{H}} \{\log [D_L(x) \cdot D_L(y)]\} + \\ & \mathbb{E}_{x \sim \mathcal{L}, y \sim \mathcal{H}} \{\log [(1 - D_H(G_L(x)))]\} + \\ & \mathbb{E}_{x \sim \mathcal{L}, y \sim \mathcal{H}} \{\log [(1 - D_L(G_H(y)))]\} \end{aligned} \quad (2)$$

The full objective function of our framework is:

$$\mathcal{L}_{total} = \lambda_{rec} \mathcal{L}_{rec} + \lambda_{adv} \mathcal{L}_{adv} \quad (3)$$

where λ_{rec} and λ_{adv} control the importance of self-reconstruction and adversarial training.

c) *Whole-slice reconstruction*:: Since the method is patch-based considering the computation complexity, we further reconstruct the whole slice from individual generated image patches. As stitching patches leads to a grid effect, we eliminate this effect by first performing histogram matching for each generated patch using the corresponding LR patches and then do median filtering as a post-processing step to remove the grid effect while preserving the structural information.

C. Bayesian Inference

To estimate the model uncertainty, we employ Monte Carlo dropout [4] to run multiple forward passes through the model using a dropout layer. To derive the uncertainty for one patch $x \in \mathcal{L}$, we collect the predictions of T inferences with different dropout masks. Let $G_L^{d_i}$ denote the generator G_L with dropout mask d_i . We obtain a sample of the possible model outputs distribution for a patch x as $\{G_L^{d_0}(x), \dots, G_L^{d_{T-1}}(x)\}$. We compute the mean and variance of this sample, corresponding to the mean of the model posterior distribution and the estimation of the model uncertainty. The predictive posterior mean p and uncertainty c are formulated as:

$$p = \frac{1}{T} \sum_{i=0}^{T-1} G_L^{d_i}; \quad c = \frac{1}{T} \sum_{i=0}^{T-1} [G_L^{d_i} - p]^2 \quad (4)$$

D. Implementation

The voxel size matching between two scanners is performed by bicubic interpolation. Each generator network contains two stride-2 convolutions, nine residual blocks [7] and two fractionally strided convolutions (1/2 stride). We use 6 blocks for the input size of $H \times W \times 1$, where H and W are the number of modalities, height and width of the images respectively. The input images and labels pass through two encoders and are merged in the last layer before the decoder. We leverage PatchGANs [8] for the discriminator network, which classifies the patch features maps to real or fake, instead of using a fully-connected layer. For training, we use the Adam optimizer with a batch size of 5 and a learning rate of 0.0001. In all experiments, we set the hyperparameters λ_{adv} and λ_{rec} to 1 and 10 respectively. We train and save the best-performing model based on the total loss. Discriminators are convolutional neural networks for binary classification. Experiments are run on one Nvidia Titan Xp GPU. The training time is eight hours. The inference stage takes 5 mins for 200 samples per patch.

E. Visual Evaluation Protocol

Due to lack of paired images, quantitative analysis of images cannot be directly performed using traditional metrics such as PSNR and SSIM [18]. Additionally these metrics

are not able to capture and evaluate useful information such as preserving the clinically relevant structures. In order to get a qualitative assessment of the images generated by our approach, we design a visual rating protocol to compare the images generated by our approach with those generated by state-of-the-art methods (i.e. using U-Net [14] and SR-GAN [9]). In each trial, the otolaryngology researchers were presented with three sets of images, with each set consisting of an original LR CT image on the left and the synthetic image generated by U-Net, SR-GAN or our approach. The rater does not know which method is used to prevent any bias. The rater is asked to rate on the following criterion: a) good resolution and low noise level and b) good shape and structural information. The otolaryngology researchers were asked to rate on a six star scale where ‘one’ represents ‘poor’ and ‘six’ represents ‘excellent’.

III. EXPERIMENTS

1) *Dataset and Evaluation Metric*: We evaluate the proposed method on a public human inner ear dataset [5] including two diverse CT scanners as shown in Table I. Specifically we perform linearly **eight times** super resolution from clinical cone beam CT to the state-of-the-art Micro CT. For pre-processing, all the low-resolution scans are matched in voxel size using bicubic interpolation and for each slice, we crop the background to obtain a region of interest by thresholding and using a bounding box. Then they are normalized using $z - score$ normalization and the intensity is then normalized to the range of $[0, 1]$ to meet the requirement of the network output. We then extract patches with a size of 256×256 from whole slices with a stride of 128 pixels resulting in a training set of 5K patches. We use six LR scans from subset ‘AL_1’ and six HR ones from subset ‘BH_1’ as a training set. Also, we use one paired scan (with same patient ID) from ‘BL_1’ and ‘AH_1’ as a test set. Note that even though the two scans are from the same patient, it is extremely difficult to align them spatially.

To quantitatively compare our method with state-of-the-art methods, we introduce *Hu Moments* (HuM) [21] as an evaluation metric on shape similarity due to its rotation- and scale- invariance in shape encoding. However, since the generated images and HR image are not aligned, it remains challenging to measure the shape similarity. Intuitively, after super resolution, the shape of the structure from two scans are expected to be similar. We propose *Maximum Hu Moments m-HuM* to handle the unpaired similarity evaluation. Given two sets of unpaired data \mathcal{X} and \mathcal{Y} , we take the maximum HuM distance for all possible combinations of the elements between the two sets:

$$m-HuM = \max\{HuM(x, y) | x \in \mathcal{X}, y \in \mathcal{Y}\} \quad (5)$$

2) *Qualitative and Quantitative Results*: We firstly evaluate our method on the test set with state-of-the-art methods U-Net [14] and SR-GAN [11]. Note that both of them are supervised-learning methods and require paired data for training. For these two methods, we synthesize LR images by bicubic interpolation considering the voxel size difference

and inject Gaussian noise as used in previous SR tasks [17]. As shown in Fig. 2, visually our method enhances the temporal bone structure and preserves good-quality shape information compared to other supervised approaches. We also observe that SR-GAN generates some artefacts in both background and structure boundary by hallucinating noisy patches which are dominated by continuous partial volume effects that are of no relevance for the bony structures, while U-NET preserves the shape structure but struggles to enhance the local structure. Although SR-GAN uses a GAN component to enhance the image quality, it does not guarantee the model can be generalized to real data. We further perform T forward passes through the model using a dropout layer to collect the predictions. In practice, we set $N = 100$ considering the computation complexity. The heatmaps in Fig. 2 depict the uncertainty obtained for the input patches. We observe that uncertainty maps match well with the temporal bone structure and thus they can serve as segmentation maps to interpret the structure in LR images.

Fig. II shows the quantitative comparison of three methods using *m-HuM*. For each whole slice, we calculate the *m-HuM* by comparing it to the whole test set. The results of all testing slices are averaged. It demonstrates that our method outperforms U-Net and SR-GAN in terms of preserving the shape of temporal bone structure.

3) *Visual Evaluations by Expert*: In order to assess how our approach generates images with clinical relevance, three raters with a mean of 7+ years of experience rated the image quality based on the criterion mentioned in Section II-E. Results on the test set for the different metrics (i.e. resolution, noise level and preservation of shape and structure) are presented in the boxplots in Fig. 3. It shows that our method outperforms U-Net and SR-GAN in both metrics. We observe that U-Net produces higher quality images than SR-GAN in terms of resolution and noise level. We conduct Wilcoxon rank-sum tests on the paired rating scores of our method and other methods from three raters on two observations (scores of three raters are averaged). Results show that the pair of metric ratings on our approach with other two methods are significantly different (with p-values < 0.0001). This demonstrates that our method significantly outperforms U-Net and SR-GAN in image quality. As claimed in Section II-A, our method benefits from learning the real distribution of LR domain instead of introducing artificial factors. This strategy strengthens the applicability of the model to real data.

IV. SUMMARY AND CONCLUSION

This work introduces a super resolution approach integrating generative adversarial network and Bayesian inference. For the first time, we address Micro-CT image synthesis in a real-world scenario using only unpaired data. This approach is potentially helpful for image-guided surgery of cochlear interventions. As a promising approach, we will investigate its usage for safer and less invasive surgical procedures. In addition, the uncertainty maps of our approach highlight

Scanner	Voxel Size (mm ³)	Volume Size	Subjects
Micro-CT	0.018 × 0.018 × 0.018	1828 × 1828 × 1828	7
cone beam CT	0.15 × 0.15 × 0.15	668 × 668 × 668	7

TABLE I: Data characteristics of a subset of the public inner ear dataset including one Micro-CT and one clinical CT.

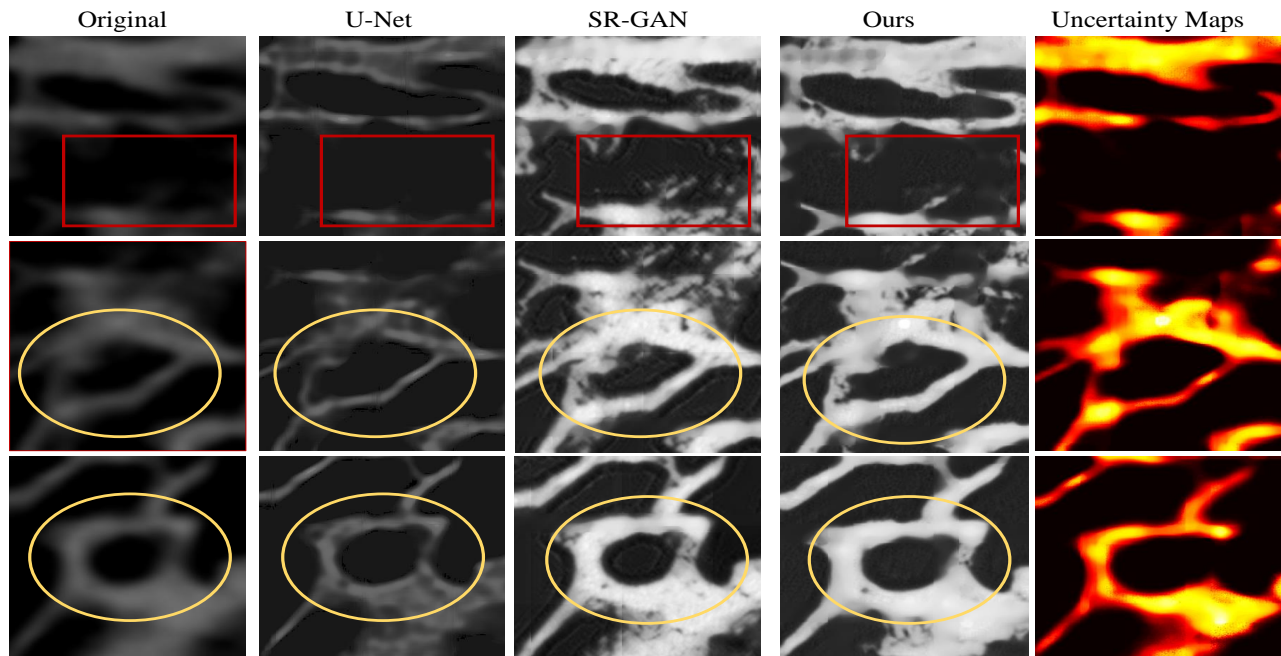


Fig. 2: Qualitative results of three approaches including our method. The region marked with red rectangle in the first row shows the artefacts generated by SR-GAN. The region marked with yellow circle shows that our approach generates good shape and local structure with less noise. The uncertainty maps highlight the structure of the temporal bone and can serve as a rough segmentation map.

Methods	U-Net [14]	SR-GAN [9]	Ours
<i>m-HuM</i> ↓	3.12	1.29	0.28

TABLE II: Comparison with state-of-the-art supervised methods using *maximum Hu Moments*. ↓ indicates that a lower value represents a higher shape similarity.

the temporal bone structure and can serve as a basis for segmentation.

V. COMPLIANCE WITH ETHICAL STANDARDS

The study was carried out in accordance with *the Declaration of Helsinki*.

VI. ACKNOWLEDGEMENT

All authors have no conflict of interest to report

REFERENCES

- [1] D. C. Alexander, D. Zikic, A. Ghosh, R. Tanno, V. Wottschel, J. Zhang, E. Kaden, T. B. Dyrby, S. N. Sotiropoulos, H. Zhang, et al. Image quality transfer and applications in diffusion mri. *NeuroImage*, 152:283–298, 2017.
- [2] K. Bahrami, F. Shi, I. Rekik, Y. Gao, and D. Shen. 7t-guided super-resolution of 3t mri. *Medical physics*, 44(5):1661–1677, 2017.

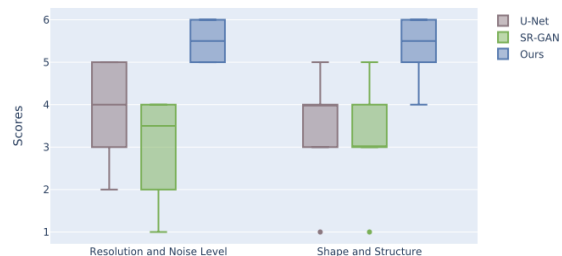


Fig. 3: Rating results by three experts. Our method generates good-quality images and significantly outperforms other supervised methods, benefiting from learning distributions on real data using GANs.

- [3] Y. Choi and et al. Stargan: Unified generative adversarial networks for multi-domain image-to-image translation. In *CVPR*, pages 8789–8797, 2018.
- [4] Y. Gal and Z. Ghahramani. Dropout as a bayesian approximation: Representing model uncertainty in deep learning. *arXiv preprint arXiv:1506.02142*, 2015.
- [5] N. Gerber, M. Reyes, L. Barazzetti, H. M. Kjer, S. Vera, M. Stauber, P. Mistrik, M. Ceresa, N. Mangado, W. Wimmer, et al. A multiscale imaging and modelling dataset of the human inner ear. *Scientific data*,

- 4:170132, 2017.
- [6] I. Goodfellow. Nips 2016 tutorial: Generative adversarial networks. *arXiv preprint arXiv:1701.00160*, 2016.
 - [7] K. He and et al. Deep residual learning for image recognition. In *CVPR*, pages 770–778, 2016.
 - [8] J. Johnson and et al. Perceptual losses for real-time style transfer and super-resolution. In *ECCV*, pages 694–711. Springer, 2016.
 - [9] C. Ledig, L. Theis, F. Huszár, J. Caballero, A. Cunningham, A. Acosta, A. Aitken, A. Tejani, J. Totz, Z. Wang, et al. Photo-realistic single image super-resolution using a generative adversarial network. In *Proceedings of the IEEE conference on computer vision and pattern recognition*, pages 4681–4690, 2017.
 - [10] H. Li, J. C. Paetzold, A. Sekuboyina, F. Kofler, J. Zhang, J. S. Kirschke, B. Wiestler, and B. Menze. Diamondgan: Unified multi-modal generative adversarial networks for mri sequences synthesis. In *International Conference on Medical Image Computing and Computer-Assisted Intervention*, pages 795–803. Springer, 2019.
 - [11] M.-Y. Liu, T. Breuel, and J. Kautz. Unsupervised image-to-image translation networks. In *Advances in neural information processing systems*, pages 700–708, 2017.
 - [12] O. Oktay, W. Bai, M. Lee, R. Guerrero, K. Kamnitsas, J. Caballero, A. de Marvao, S. Cook, D. O’Regan, and D. Rueckert. Multi-input cardiac image super-resolution using convolutional neural networks. In *International conference on medical image computing and computer-assisted intervention*, pages 246–254. Springer, 2016.
 - [13] J. Park, D. Hwang, K. Y. Kim, S. K. Kang, Y. K. Kim, and J. S. Lee. Computed tomography super-resolution using deep convolutional neural network. *Physics in Medicine & Biology*, 63(14):145011, 2018.
 - [14] O. Ronneberger, P. Fischer, and T. Brox. U-net: Convolutional networks for biomedical image segmentation. In *International Conference on Medical image computing and computer-assisted intervention*, pages 234–241. Springer, 2015.
 - [15] W. Shi, J. Caballero, C. Ledig, X. Zhuang, W. Bai, K. Bhatia, A. M. S. M. de Marvao, T. Dawes, D. O’Regan, and D. Rueckert. Cardiac image super-resolution with global correspondence using multi-atlas patchmatch. In *International Conference on Medical Image Computing and Computer-Assisted Intervention*, pages 9–16. Springer, 2013.
 - [16] R. Tanno, D. E. Worrall, A. Ghosh, E. Kaden, S. N. Sotiropoulos, A. Criminisi, and D. C. Alexander. Bayesian image quality transfer with cnns: exploring uncertainty in dmri super-resolution. In *International Conference on Medical Image Computing and Computer-Assisted Intervention*, pages 611–619. Springer, 2017.
 - [17] Z. Wang, J. Chen, and S. C. Hoi. Deep learning for image super-resolution: A survey. *arXiv preprint arXiv:1902.06068*, 2019.
 - [18] P. Welander, S. Karlsson, and A. Eklund. Generative adversarial networks for image-to-image translation on multi-contrast mr images—a comparison of cyclegan and unit. *arXiv preprint arXiv:1806.07777*, 2018.
 - [19] M. Yurt, S. U. H. Dar, A. Erdem, E. Erdem, and T. Çukur. mustgan: Multi-stream generative adversarial networks for mr image synthesis. *arXiv preprint arXiv:1909.11504*, 2019.
 - [20] J.-Y. Zhu and et al. Unpaired image-to-image translation using cycle-consistent adversarial networks. In *CVPR*, pages 2223–2232, 2017.
 - [21] J. Žunić, K. Hirota, and P. L. Rosin. A hu moment invariant as a shape circularity measure. *Pattern Recognition*, 43(1):47–57, 2010.